

HI 21cm absorption at $z \sim 2.347$ towards PKS B0438–436

N. Kanekar^{1*}, R. Subrahmanyan², S. L. Ellison³, W. M. Lane⁴, J. N. Chengalur^{2,5}

¹National Radio Astronomy Observatory, Socorro, NM 87801, USA; ²Australia Telescope National Facility, Epping, Australia; ³University of Victoria, BC, Canada; ⁴US Naval Research Laboratory, Washington, USA; ⁵National Centre for Radio Astrophysics, Pune, India

Received mmdyy/ accepted mmdyy

ABSTRACT

We report the detection of redshifted HI 21cm absorption in the $z \sim 2.347$ damped Lyman- α absorber (DLA) towards PKS B0438–436, with the Green Bank Telescope. This is the second-highest redshift at which 21cm absorption has been detected in a DLA. The absorption extends over $\sim 60 \text{ km s}^{-1}$ and has two distinct components, at $z = 2.347477(12)$ and $z = 2.347869(20)$. A similar velocity structure is seen in optical metal lines, although the peak absorption here is offset by $\sim 11 \text{ km s}^{-1}$ from the peak in the 21cm line. We obtain a high spin temperature $T_s \sim (886 \pm 248) \times (f/0.58) \text{ K}$, using a covering factor estimated from 2.3 GHz VLBI data. However, the current data cannot rule out a low spin temperature. The non-detection of CO 3–2 absorption places the upper limit $N_{\text{CO}} < 3.8 \times 10^{15} \times (T_x/10) \text{ cm}^{-2}$ on the CO column density.

Key words: galaxies: high redshift – galaxies: ISM – radio lines: galaxies

1 INTRODUCTION

The highest HI column density absorption systems in quasar spectra, the damped Lyman- α absorbers (DLAs), are important in the context of galaxy evolution as they are believed to be the precursors of present-day galaxies (Wolfe et al. 1986). Understanding the nature of a typical DLA and its evolution with redshift is perhaps the key to understanding normal galaxy evolution. However, despite a tremendous observational effort over the last two decades, physical conditions in high z DLAs are still the subjects of much debate (see Wolfe et al. (2005) for a recent review).

HI 21cm absorption studies of DLAs towards radio-loud background sources provide crucial information on the nature of the absorbing galaxy (e.g. Kanekar & Briggs 2004). 21cm lines are usually optically thin and trace the kinematics of the neutral gas; they can thus be used to obtain the velocity field of the absorber and its HI and dynamical masses (Briggs et al. 2001). In some cases, the gas kinetic temperature can be directly measured with high resolution 21cm spectroscopy (e.g. Lane et al. 2000). Comparisons between the redshifts of 21cm and metal-line or molecular absorption allow estimates of changes in fundamental constants (e.g. Tzanavaris et al. 2005). Finally, the 21cm equivalent width can be combined with the HI column density to obtain the spin temperature T_s of the absorbing gas (e.g. Kanekar & Chengalur 2003); this contains information on the distribution of the HI between phases at different temperatures, one of the issues of controversy referred to above (Kanekar & Chengalur 2003; Wolfe et al. 2003).

A problem with using 21cm absorption to probe physical

conditions in high z DLAs is that there are, at present, only three absorbers in the literature with confirmed detections of absorption at $z > 1$ (Wolfe & Davis 1979; Wolfe & Briggs 1981; Wolfe et al. 1985), with one further tentative detection at $z \sim 3.38$ (Briggs et al. 1997). Despite deep searches, the vast majority of systems only yield upper limits on T_s (e.g. Kanekar & Chengalur 2003). This is very different from the situation at low redshifts, $z \lesssim 0.8$, where 14 intervening 21cm absorbers are known (e.g. Brown & Roberts 1973; Kanekar & Chengalur 2001; Lane & Briggs 2002). We have therefore been carrying out deep searches for 21cm absorption in a large sample of high redshift DLAs with the Green Bank Telescope (GBT) and report here the detection of a new 21cm absorption system in the $z \sim 2.347$ DLA towards the $z \sim 2.863$ QSO, PKS 0438–436 (Ellison et al. 2001).

2 OBSERVATIONS AND DATA ANALYSIS

The initial GBT observations of PKS B0438–436 were carried out in January 2004, with the PF1-450 MHz receiver. These used the GBT Spectral Processor as the backend, with two linear polarizations and a 5 MHz bandwidth centred at 424.5 MHz and sub-divided into 1024 channels (giving a velocity resolution of $\sim 6.9 \text{ km s}^{-1}$, after Hanning smoothing). A standard “position-switched” mode was used, with ten-minute On-Off cycles made up of ten-second integrations. System temperatures were measured during the observations using a noise diode. The total on-source time was 30 minutes.

These observations resulted in the tentative detection of an absorption feature at $\sim 424.32 \text{ MHz}$, close to the expected redshifted line frequency. We hence re-observed PKS B0438–436 in August 2005 to confirm the absorption, at higher spectral resolu-

* E-mail: nkanekar@aoc.nrao.edu (NK); rsubrahm@rri.res.in (RS); sarae@uvic.ca (SLE); wendy.peters@nrl.navy.mil (WML); chengalur@ncra.tifr.res.in (JNC)

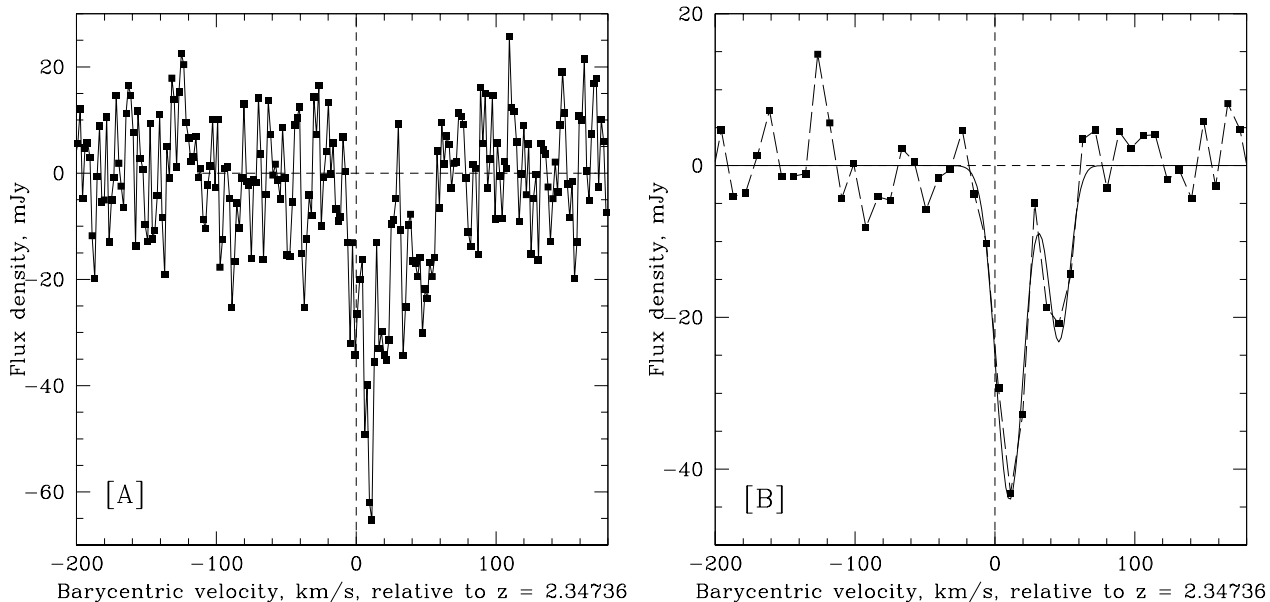


Figure 1. Final GBT HI 21cm spectrum towards PKS B0438–436 from August 2005, with flux density (in mJy) plotted against barycentric velocity (in km/s), relative to $z = 2.34736$. [A]: The spectrum at the original resolution of 1.73 km s^{-1} . [B]: The spectrum (dashed line) and 2-gaussian fit (solid line) after smoothing by 5 channels (and resampling) to a resolution of $\sim 8.6 \text{ km s}^{-1}$. The QSO continuum flux density has been subtracted from both spectra.

tion. The observing and data recording procedures were the same as those of January 2004, except that a bandwidth of 1.25 MHz, centred at 424.3 MHz was used, sub-divided into 1024 channels (i.e. a spectral resolution of $\sim 1.73 \text{ km s}^{-1}$, after Hanning smoothing). The total on-source time was 80 minutes.

The data were analysed in the AIPS++ single dish package DISH, using standard procedures. No radio frequency interference (RFI) was found at or near the expected line frequency. After initial data-editing, the spectra were calibrated and averaged together, to measure the flux density of the background quasar, using a telescope gain of 2 K/Jy . This gave flux densities of $7.5 \pm 0.7 \text{ Jy}$ in January 2004 and $7.1 \pm 0.7 \text{ Jy}$ in August 2005, at 424 MHz, where the errors include those from confusing sources in the primary beam; (for comparison, Large et al. (1981) obtain $8.12 \pm 0.25 \text{ Jy}$ at 408 MHz). A second-order spectral baseline was then fit to each 10-second spectrum (during the process of calibration) and subtracted out; the frequency range covered in the fit was $\sim 423.7 - 424.7 \text{ MHz}$, for both data sets. The residual 10-second spectra were then averaged together, to produce a spectrum for each epoch. The August 2005 spectrum was found to not be entirely flat at the end of this procedure; a second order polynomial was hence fit to this spectrum, excluding line channels, and subtracted out to produce the final spectrum. This has a higher sensitivity, a finer resolution and a better spectral baseline than the spectrum of January 2004, and will therefore be used as the final 21cm spectrum towards PKS B0438–436 in the discussion below.

We also carried out a search for redshifted CO 3–2 absorption from the $z \sim 2.347$ DLA with the 3-mm receivers of the Australia Telescope Compact Array (ATCA), in October 2005. The antennas were in the EW214 configuration, with a longest baseline of 214 m. A bandwidth of 64 MHz was used for the observations, centred at 103.315 GHz and divided into 128 channels; this gave dual linear polarization spectra with an effective velocity resolution of 1.77 km s^{-1} . The observations consisted of 10-minute scans on PKS B0438–436, interleaved with 2-minute scans on the bright

nearby source PKS B0454–463. The telescope pointing and system temperature calibrations were updated every hour; we obtained above-atmosphere T_{sys} in the range 300–350 K in the different antennas, at the observing frequency. The planet Mars was observed at the start of the run to calibrate the absolute flux density scale. The total on-source time was 210 minutes.

The ATCA data were analysed in the software package MIRIAD, using standard procedures. The complex gains and bandpass shapes of the ATCA antennas were derived from the visibility data on PKS B0454–463 while the flux density scale was bootstrapped using the visibility amplitudes on Mars measured on the shortest (30-m) baseline (Mars is resolved on the longer ATCA baselines). The channel velocities towards PKS B0438–436 were then shifted to the barycentric frame and the calibrated visibilities averaged to derive the final spectra. The source flux density was measured to be 0.36 Jy , at a frequency of 103 GHz.

3 SPECTRA AND RESULTS

The final redshifted HI 21cm spectrum towards PKS B0438–436 from August 2005 is shown in Figs. 1[A] and [B], with flux density (in mJy) plotted against barycentric velocity (in km/s), relative to $z = 2.34736$, the redshift of the strongest metal line absorption (Akerman et al. 2005). We adopt this as the systemic redshift of the DLA, indicated by the dashed vertical lines in the two panels of the figure. Fig. 1[A] shows the HI spectrum at the original velocity resolution of $\sim 1.73 \text{ km s}^{-1}$, with an RMS noise of $\sim 10.4 \text{ mJy}$ per channel, while Fig. 1[B] shows the spectrum smoothed by 5 channels (and resampled), at a final resolution of $\sim 8.6 \text{ km s}^{-1}$, with an RMS noise of $\sim 4.7 \text{ mJy}$ per resampled channel.

The stronger 21cm component of Fig. 1[B] is clearly detected in both observing runs, with the correct Doppler shift due to the Earth’s motion; there is no doubt about its reality. While the weaker 21cm component (at $\sim +45 \text{ km s}^{-1}$) was only detected in the

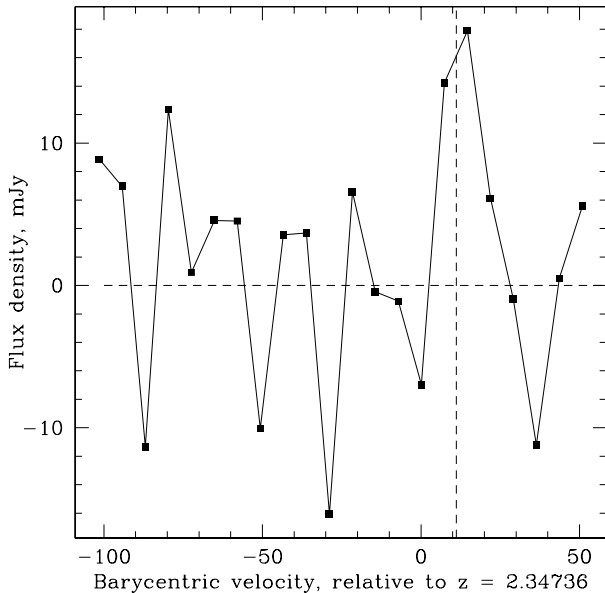


Figure 2. ATCA 13 km s^{-1} resolution CO 3–2 spectrum towards PKS B0438–436, with flux density (in mJy) plotted against barycentric velocity (in km s^{-1}), relative to $z = 2.34736$. The QSO flux density has been subtracted from the spectrum. The dashed vertical line shows the CO 3–2 frequency corresponding to the peak 21cm line redshift.

higher sensitivity spectrum of August 2005, the data showed no evidence for RFI and the feature is detected at $> 5\sigma$ level. Moreover, as we will discuss later, both the redshift and the velocity width of this feature are in excellent agreement with those of a component detected in the FeII $\lambda 2374$ transition. We conclude that the second 21cm component is also likely to be real.

The 21cm absorption towards PKS B0438–436 extends, between nulls, over $\sim 60 \text{ km s}^{-1}$, with an equivalent width of $\sim (0.216 \pm 0.027) \text{ km s}^{-1}$. The solid line in Fig. 1[B] shows a two-component fit to the spectrum, with the components modelled as Gaussians. The peak redshifts of the components are $z_1 = 2.347477(12)$ and $z_2 = 2.347869(20)$ and their peak optical depths (the ratio of line depth to continuum flux density, using the low optical depth limit; PKS B0438–436 is unresolved by the GBT beam) are $\tau_1 = (6.2 \pm 0.8) \times 10^{-3}$ and $\tau_2 = (3.3 \pm 0.7) \times 10^{-3}$ (including errors in the source flux density). They have fairly large velocity spreads (FWHMs of $\sim (23.3 \pm 2.7) \text{ km s}^{-1}$ and $\sim (18.2 \pm 4.5) \text{ km s}^{-1}$, respectively), suggesting either a blend of many cold narrow components or that bulk/turbulent motions are important. Alternatively, if the absorption arises in a warm phase, with the velocity spread primarily due to thermal motions, the implied kinetic temperatures of the two components are $\lesssim (11865 \pm 2750) \text{ K}$ and $\lesssim (7240 \pm 3580) \text{ K}$.

Fig. 2 shows the final ATCA redshifted CO 3–2 spectrum towards PKS B0438–436, with flux density, in mJy, plotted against barycentric velocity, in km s^{-1} , relative to $z = 2.34736$; the dashed line indicates the peak of the 21cm absorption. The spectrum has been smoothed to (and resampled at) a velocity resolution of $\sim 7.25 \text{ km s}^{-1}$ and shows no evidence for absorption, with an RMS noise of $\sim 8.6 \text{ mJy per } 7.25 \text{ km s}^{-1}$. The 3σ upper limit on the optical depth is $\tau < 0.058$, per $\sim 10.2 \text{ km s}^{-1}$. Curiously, however, a weak emission feature can be seen in the spectrum at the redshifted CO 3–2 frequency. While this has only $\sim 3\sigma$ significance in a single channel (after smoothing by 3 channels and

resampling), it is somewhat tantalizing, especially as it is present (albeit at even weaker levels) in the two independent polarizations and occurs at the 21cm redshift. We discuss the implications of a positive detection in the next section.

4 DISCUSSION

For optically thin 21cm absorption, the HI column density N_{HI} (in cm^{-2}), 21cm optical depth τ_{21} and spin temperature T_s (in K) are related by the equation

$$N_{\text{HI}} = 1.823 \times 10^{18} [\tau_{21}/f] \int \tau_{21} dV, \quad (1)$$

where the profile integral is over velocity (in km s^{-1}) and the covering factor f gives the fraction of the radio source that is obscured by the foreground cloud. The detection of 21cm absorption in a DLA, where the HI column density is known from the Lyman- α line, thus allows an estimate of the spin temperature of the absorbing gas (assuming that the HI column density measured towards the optical QSO is the same as that towards the radio source). As has often been emphasized (e.g. Carilli et al. 1996; Chengalur & Kanekar 2000), the spin temperature thus obtained is the column-density-weighted harmonic mean of the spin temperatures of different HI phases along the line of sight. In the case of the $z \sim 2.347$ DLA, the HI column density is $N_{\text{HI}} = (6 \pm 1.5) \times 10^{20} \text{ cm}^{-2}$ (Ellison et al. 2001). The measured 21cm equivalent width of $\int \tau_{21} dV = (0.216 \pm 0.027) \text{ km s}^{-1}$ then yields $T_s = [(1527 \pm 428) \times f] \text{ K}$, where the error is dominated by the uncertainty in N_{HI} .

In order to estimate the covering factor, it is important to first determine whether both 21cm absorption components of Fig. 1[B] arise against the quasar core. Figs. 3[A] and [B] show a comparison between the HI 21cm profile (histogram) and the FeII $\lambda 2374$ and ZnII $\lambda 2062$ profiles of Akerman et al. (2005). The FeII and 21cm profiles are similar, with FeII absorption seen at the velocities of both 21cm components; this suggests that the latter indeed arise from the line of sight towards the optical nucleus.

The covering factor f can thus be assumed to be the fraction of source flux density contained in the core and is best estimated from VLBI observations of the radio source at the redshifted 21cm line frequency; unfortunately, no such observations of PKS B0438–436 exist in the literature. The lowest frequency with published VLBI observations is 2.3 GHz, where most of the source flux density stems from two compact components, separated by 35 mas (Preston et al. 1989). Of these, the northwest component is more compact than the southeast one ($\sim 5 \text{ mas v/s } \sim 18 \text{ mas}$) and is likely to be the nuclear core, especially since it is also very compact in higher resolution ($\lesssim 2 \text{ mas}$) 4.8 GHz VLBI and VSOP images (Shen et al. 1998; Tingay et al. 2002). The core has a flux density of $\sim 2.5 \text{ Jy}$ in the 2.3 GHz VLBI image, $\sim 58\%$ of the total 2.3 GHz flux density (Preston et al. 1989). Unfortunately, the source is highly variable and it is thus not possible to determine its spectral index or its core flux density at 424.3 MHz from the 2.3 and 4.8 GHz VLBI data, as these observations were carried out at very different epochs, many years before our observations. For now, we are forced to estimate the covering factor solely from the 2.3 GHz VLBI information. Assuming that only the core is completely covered gives $f = 0.58$ from the 2.3 GHz data, and, hence, a high spin temperature, $T_s = (886 \pm 248) \text{ K}$. Of course, it is quite possible that both 2.3 GHz source components are covered by the DLA, since their separation of 35 mas corresponds to a lin-

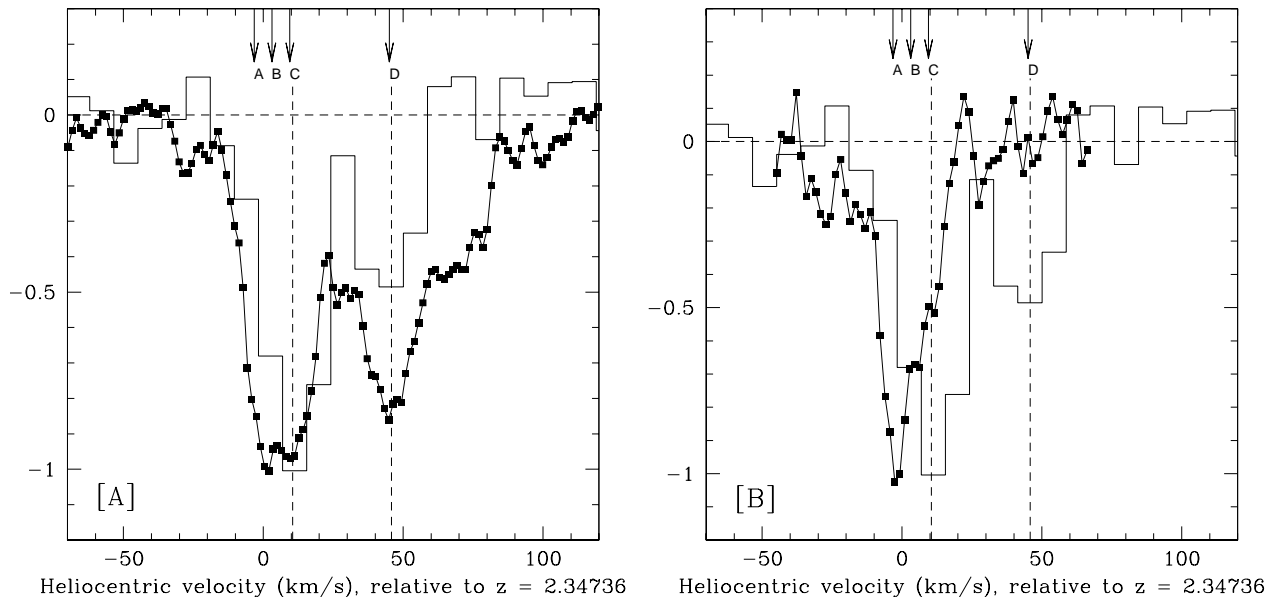


Figure 3. A comparison between the GBT HI 21cm profile of Fig. 1[B] (histogram) and the [A] FeII $\lambda 2374$ and [B] ZnII $\lambda 2062$ profiles (solid points), with all spectra in arbitrary units. The redshifts of the two 21cm components are shown by the two dashed vertical lines while the arrows at the top of each panel (marked A, B, C and D) indicate the 4 FeII components of Table 1. See text for discussion.

| | Velocity km s ⁻¹ | Redshift z | b km/s | N _{FeII} cm ⁻² | N _{ZnII} cm ⁻² | [Zn/Fe] |
|---|--------------------------------|---------------|-----------|---------------------------------------|---------------------------------------|---------|
| A | -3.2 | 2.347324 | 1.0 | 14.58 | 12.07 | 0.33 |
| B | +3.1 | 2.347395 | 9.0 | 14.23 | 12.54 | 1.15 |
| C | +9.5 | 2.347466 | 9.3 | 14.34 | 11.83 | 0.33 |
| D | +45.1 | 2.347864 | 11.3 | 14.28 | < 11.7 | < 0.26 |

Table 1. The FeII and ZnII column densities and [Zn/Fe] for the four strongest FeII components (in logarithmic units), with the [Zn/Fe] values relative to the solar abundances of Lodders (2003). Components C and D have velocities in good agreement with those of the 21cm components.

ear scale of only ~ 290 pc at $z = 2.347$ (using an LCDM cosmology, with $\Omega_m = 0.3$, $\Omega_\Lambda = 0.7$ and $H_0 = 70$ km/s Mpc⁻¹). In such a situation, with $f \sim 1$, the spin temperature would be even higher, $T_s \sim (1527 \pm 428)$ K. Conversely, it is possible that the spin temperature is significantly lower than this, if the core has an inverted spectrum and is the only source component covered by the DLA. We note that the other confirmed $z > 1$ HI 21cm absorbers, in the DLAs towards QSO 1331+170, PKS 1157+014 and PKS 0458-020, also have relatively high spin temperatures, $T_s \gtrsim 500$ K (e.g. Kanekar & Chengalur 2003).

The average metallicity of the $z \sim 2.347$ DLA is quite high for these redshifts, $[\text{Zn}/\text{H}] = -0.68 \pm 0.15$ (Akerman et al. 2005). Of course, the lack of velocity information in the Lyman- α line precludes measurements of the HI column densities (and hence, the metallicities) of individual absorption components. We have used VPFIT to fit the ZnII and FeII transitions detected in the VLT-UVES spectrum of Akerman et al. (2005); this has a resolution of ~ 7 km s⁻¹ and S/N ~ 25 near the ZnII and FeII wavelengths. Table 1 lists the velocities (relative to $z = 2.34736$), redshifts, b -parameters, FeII and ZnII column densities and the dust depletion (as measured by [Zn/Fe]) of the four strongest components in the DLA, obtained from the fits. The first three components (A – C) in the table contribute to the strongest optical absorption (peaking at

$v \sim 0$ km s⁻¹ in Fig. 3, ~ 11 km s⁻¹ blueward of the stronger 21cm absorption), while the fourth is associated with the weaker 21cm absorption, at $v \sim 45$ km s⁻¹. The weaker 21cm component is not detected in the ZnII lines; 3σ upper limits on its ZnII column density and dust depletion are listed in Table 1. Although the optical absorption has been decomposed into sub-components during the fitting procedure, the modest S/N of the UVES spectrum and the complex kinematics of the metal lines introduce a considerable amount of degeneracy. Errors on the column densities and redshifts of individual components are therefore sizable. However, the total column densities are well constrained, with our values in excellent agreement with those of Akerman et al. (2005), despite the very different fits. We hence combine the three optical components at $v \sim 0$ km s⁻¹ to obtain $[\text{Zn}/\text{Fe}] = (0.62 \pm 0.14)$, indicating a fairly high dust depletion compared to other DLAs at this redshift. Conversely, the component at $v \sim 45$ km/s has a much lower implied dust-to-gas ratio, $[\text{Zn}/\text{Fe}] < 0.26$. Fig. 8[A] of Wolfe et al. (2005) shows that all DLAs with $[\text{Zn}/\text{Fe}] < 0.4$ have $[\text{Zn}/\text{H}] \lesssim -1$. Although this result is obtained from [Zn/H] and [Zn/Fe] values averaged over the entire profile (i.e. not from individual components), it suggests that the $v \sim 45$ km s⁻¹ gas has a low metallicity. The $v \sim 0$ km s⁻¹ gas should then have a fairly high metallicity, to account for the high average metallicity of the absorber. The DLA thus appears to contain some gas that is rich in dust and metals and with a relatively large 21cm optical depth, as well as a second component that is poorer in heavier elements and with weaker 21cm absorption. The very different depletions seen in the two components imply that the absorber has a rather non-uniform interstellar medium, as recently seen in other high z DLAs (Dessauges-Zavadsky et al. 2006). In fact, the FeII $\lambda 2374$ and ZnII $\lambda 2062$ lines at $v \sim 0$ km s⁻¹ have quite different shapes, suggesting that even the sub-components within this complex have significantly different physical conditions.

Comparisons between 21cm and optical redshifts in a statistically large absorber sample can be used to probe the evolution

of fundamental constants (Wolfe et al. 1976). The most sensitive result is that of Tzanavaris et al. (2005), who compare the redshifts of strongest 21cm and metal-line absorption in 8 DLAs to constrain changes in the quantity $x \equiv g_p \mu \alpha^2$, where α is the fine structure constant, g_p , the proton gyro-magnetic ratio and $\mu \equiv m_e/m_p$, the electron-proton mass ratio. However, it is by no means essential that the strongest 21cm and metal absorption both arise from the same absorption component; for example, Chengalur & Kanekar (2000) noted that the deepest UV absorption in the $z \sim 2.04$ DLA towards PKS 0458–020 is offset from the strongest 21cm component but in good alignment with the secondary 21cm component. Similarly, both panels of Fig. 3 show that the strongest optical absorption in PKS B0438–436 (at $z \sim 2.347360$) is offset from the strongest 21cm absorption by $\sim 11 \text{ km s}^{-1}$. In the approach of Tzanavaris et al. (2005), these offsets would imply either evolution in the fundamental constants or an intrinsic velocity offset between the 21cm and metal lines. However, it can be seen from Fig. 3[A] and Table 1 that there are weaker FeII components (C and D) in PKS B0438–436 much closer to the redshifts of both 21cm components. While component C (at $v = +9.5 \text{ km s}^{-1}$) is severely blended with the complex at $v \sim 0 \text{ km s}^{-1}$, making it difficult to determine an accurate redshift from the present spectrum, the fit to component D at $v \sim +45 \text{ km s}^{-1}$ is quite stable, yielding the redshift $z_1 = 2.347864(5)$ (note that the RMS-error of the wavelength solution is $\sim 250 \text{ m s}^{-1}$, a factor of two smaller than the error from the fit). Comparing this to the redshift of the nearest (weaker) 21cm component, $z_2 = 2.347869(20)$ (from the 2-gaussian fit), we obtain $[\Delta x/x] = \Delta z/(1 + \bar{z}) = (-0.15 \pm 0.62) \times 10^{-5}$, where $\Delta z = z_1 - z_2$ and \bar{z} is the mean of the redshifts; this is consistent with the null result of no evolution. Note that this error does not include possible systematic velocity offsets between the 21cm and UV redshifts, which can only be addressed with statistically large samples. However, it is clear that the results obtained from such comparisons between different species (and using lines at very different wavelengths) critically depend on the precise details of the comparison. The assumption that the strongest absorption in the two species arises in the same component introduces an extra source of error, that could well dominate the $\sim 6 \text{ km s}^{-1}$ “intrinsic” offset between 21cm and UV redshifts obtained by Tzanavaris et al. (2005), leading to a bias in favour of a detection (especially in small samples). It may thus be better to compare the redshifts of the *nearest* simple (i.e. unblended) metal and 21cm components, after using high resolution spectroscopy to decompose the profiles into their components, as has been done here. While this might have the opposite bias, towards a non-detection of evolution, it could be considered a test of the null hypothesis. In any case, care must be taken in the interpretation of the results from such comparisons.

The ATCA non-detection of CO 3–2 absorption in Fig. 2 places limits on the CO column density in the $z \sim 2.347$ DLA. Assuming a velocity width of 10 km s^{-1} gives the 3σ limit $N_{\text{CO}} < 3.8 \times 10^{15} \times (T_x/10) \text{ cm}^{-2}$, similar to earlier limits in DLAs (e.g. Curran et al. 2004). A conversion factor of 10^5 from N_{CO} to N_{H_2} (Liszt & Lucas 2000) gives $N_{\text{H}_2} < 3.8 \times 10^{20} \times (T_x/10) \text{ cm}^{-2}$, i.e. a molecular fraction $f < 0.6$.

The possible CO 3–2 emission feature seen in Fig. 2, if real, corresponds to a molecular mass of $M_{\text{H}_2} \sim 4.2 \times 10^{10} M_\odot$, an exceedingly large value (using the Galactic conversion factor of $4.6 M_\odot (\text{K km/s pc}^2)^{-1}$ from the CO line luminosity L'_{CO} to mass; Solomon et al. 1997). CO emission has never before been detected from a DLA. We note that the velocity width of the feature is quite narrow, $\sim 30 \text{ km s}^{-1}$; if real, this would be surprising for

such a large molecular mass and would require the galaxy to be quite close to face-on to the line of sight.

In summary, we have used the GBT to detect HI 21cm absorption in the $z \sim 2.347$ DLA towards PKS B0438–436. We obtain a high spin temperature $T_s = (886 \pm 248) \times (f/0.58) \text{ K}$, estimating the covering factor f from 2.3 GHz VLBI observations.

Acknowledgements

We thank Bob Garwood for much help with the AIPS++ data analysis and Carl Bignell and Toney Minter for help with the GBT observations. Basic research in radio astronomy at the Naval Research Laboratory is funded by the Office of Naval Research. The NRAO is operated by Associated Universities, Inc., under cooperative agreement with the National Science Foundation. The ATCA is part of the Australia Telescope, funded by the Commonwealth of Australia for operation as a National Facility managed by CSIRO.

REFERENCES

- Akerman C. J., Ellison S. L., Pettini M., Steidel C. C., 2005, *A&A*, 440, 499
 Briggs F. H., Brinks E., Wolfe A. M., 1997, *AJ*, 113, 467
 Briggs F. H., de Bruyn A. G., Vermeulen R. C., 2001, *A&A*, 373, 113
 Brown R. L., Roberts M. S., 1973, *ApJ*, 184, L7
 Carilli C. L., Lane W. M., de Bruyn A. G., Braun R., Miley G. K., 1996, *AJ*, 111, 1830
 Chengalur J. N., Kanekar N., 2000, *MNRAS*, 318, 303
 Curran S. J., Murphy M. T., Pihlström Y. M., Webb J. K., Bolatto A. D., Bower G. C., 2004, *MNRAS*, 352, 563
 Dessauges-Zavadsky M., Prochaska J. X., D’Odorico S., Calura F., Matteucci F., 2006, *A&A*, 445, 93
 Ellison S. L., Yan L., Hook I. M., Pettini M., Wall J. V., Shaver P., 2001, *A&A*, 379, 393
 Kanekar N., Briggs F. H., 2004, *New Astr. Rev.*, 48, 1259
 Kanekar N., Chengalur J. N., 2001, *A&A*, 369, 42
 Kanekar N., Chengalur J. N., 2003, *A&A*, 399, 857
 Lane W. M., Briggs F. H., 2002, *ApJ*, 561, L27
 Lane W. M., Briggs F. H., Smette A., 2000, *ApJ*, 532, 146
 Large M. I., Mills B. Y., Little A. G., Crawford D. F., Sutton J. M., 1981, *MNRAS*, 194, 693
 Liszt H., Lucas R., 2000, *A&A*, 355, 333
 Ladders K., 2003, *ApJ*, 591, 1220
 Preston R. A., Jauncey D. L., Meier D. L., et al. 1989, *AJ*, 98, 1
 Shen Z.-Q., Wan T.-S., Moran J. M., et al. 1998, *AJ*, 115, 1357
 Solomon P. M., Downes D., Radford S. J. E., Barrett J. W., 1997, *ApJ*, 478, 144
 Tingay S. J., Reynolds J. E., Tzioumis A. K., Jauncey D. L., et al. 2002, *ApJS*, 141, 311
 Tzanavaris P., Webb J. K., Murphy M. T., Flambaum V. V., Curran S. J., 2005, *Phys. Rev. Lett.*, 95, 041301
 Wolfe A. M., Briggs F. H., 1981, *ApJ*, 248, 460
 Wolfe A. M., Briggs F. H., Turnshek D. A., Davis M. M., Smith H. E., Cohen R. D., 1985, *ApJ*, 294, L67
 Wolfe A. M., Brown R. L., Roberts M. S., 1976, *Phys. Rev. Lett.*, 37, 179
 Wolfe A. M., Davis M. M., 1979, *AJ*, 84, 699
 Wolfe A. M., Gawiser E., Prochaska J. X., 2003, *ApJ*, 593, 235
 Wolfe A. M., Gawiser E., Prochaska J. X., 2005, *ARA&A*, 43, 861

6 *Kanekar et al.*

Wolfe A. M., Turnshek D. A., Smith H. E., Cohen R. D., 1986,
ApJS, 61, 249